15 Global Climate Scenarios: conversion to *netCDF* and inter-comparisons.

R.E. Benestad

DNMI, June 12, 2001

Klima: 16/00

Contents

1 Introduction

This report aims to document the conversion of the global IPCC climate scenarios to the netCDF (*Rew* et al., 1996) format. The conversion code (asc2ncdf.sh, see Appendix A) was developed by R.E. Benestad, and is written in FORTRAN90. It takes the ASCII formatted data from the IPCC web site (year 2000: http://ipcc-ddc.cru.uea.ac.uk/dkrz/dkrz_index.html) as input (There were some problems with reading the GRIB format (*Dey*, 1998), there was a conflict between the GRIB and netCDF FORTRAN libraries, and it was easier and quicker to read the ASCII format) and save as netCDF. The choice of converting to netCDF is that this format is more easily accessible than either GRIB or ASCII in terms of geophysical graphics packages (eg Ferret, ncview) as well as numerical tools (eg Matlab, IDL). There is no need for looking up codes or knowing how to decode the (GRIB) data and there is no need for scanning the data files to create index files. Furthermore, only one application is needed to read all netCDF files, whereas many different versions of the application are required for reading all the scenarios in ASCII and GRIB (with the exception of GrADS and Metview). The netCDF format is platform independent (no need for byte swapping) and allows direct access. it also gives data file sizes of similar order to the GRIB format.

Here only the monthly mean near-surface (2-meter for most models, but 1.5-meter for HadCM3, the lowest level temperature which is sigma 0.99 for the GFDL model) temperature and the sea level pressure (SLP) were converted to netCDF.

Simple quality control was applied to the converted data. Such tests included a visual inspection of the mean fields and the variance, a comparison between the North Atlantic Oscillation indices (NAOI) and the Southern Oscillation indices from the various models. Further analysis was applied to the atmosphere-ocean general circulation (AOGCM) results to check that these gave a realistic description of the near-surface coupling between thermodynamic and dynamic processes.

It took approximately a week to convert the IPCC scenarios and check the conversion.

2 Method

The conversion code used the 2-byte short (NF_SHORT/NCSHORT) type for saving the bulk of the data, and a scale factor and an offset were used to scale the data appropriately so that the information was stored with a minimal loss of information. This choice implied rounding off the data to

Table 1: *Examples of configuration types*

```
asc2ncdf.sh
asc2ncdf CSGS_tas__1881-1889.mon > test
asc2ncdf CSGS_tas__1890-1899.mon > test
asc2ncdf CSGS_tas__1900-1909.mon > test
.
.
asc2ncdf CSGS_tas__2100-2100.mon > test
```

the nearest 0.01 hPa or degree K. The reason for using the short type was to reduce the file size. The data files were stored following the standard netCDF convention (*Rew* et al., 1996, chap. 8.1).

The FORTRAN code itself was based on the codes used by *Benestad* (1999b) and *Benestad* (1999a), but was modified to read ASCII files as there appears to be a conflict between the GRIB and netCDF libraries (the previous conversions were done in two steps: first convert the GRIB data to binary, then convert the binary files to netCDF). The netCDF files require much less space than the ASCII files, which were unnecessarily large since each datum was stored as 14-character floating point number (14 bytes, see appendix D) as opposed to being represented by a scaled integer.

The conversion code is executed once for each ASCII file, and the code searches the directory to see if the netCDF file already exists. If so, the code appends the already existing file. The time information is based on the first year (eg. 1881) in the original file name, but the sequence of the data is determined by the order of conversion. It is therefore important to convert the files in chronological order and not repeat the conversion of the same file.

Table 2 shows how the conversion code is done manually: *compile the code by calling the script asc2ncdf.sh, and then convert the data by running the executable (asc2ncdf) with the filename of the ASCII file as one argument.* The netCDF filename is determined automatically by the code (based on the ASCII data filename).

Two UNIX shell scripts were written to retrieve and convert all the time slices more easily: *getippc.sh* and *convertall.sh*. The former downloads all the files in the given directory (the path name must be set specifically for the particular scenario to be retrieved) whereas the latter decompresses the data files, converts them to netCDF, and then removes the "used" ASCII files. It is a good idea to make a test conversion of the first ASCII file manually using the *asc2ncdf* executable to ensure that the data information and the grid (latitudes) are correct. It is important to remove the netCDF file from this test before executing *convertall.sh*, otherwise the code will just add the

Table 2: *Data retrieval using old fashion FTP*

```
saragasso 694Connected to ftp.dkrz.de.
.
.
Name (ftp.dkrz.de:kareb): anonymous
.
.
230 Guest login ok, access restrictions apply.
Remote system type is UNIX.
Using binary mode to transfer files.
ftp> cd pub/ipcc/ddc/gzip/HadleyCM3/all/temk
ftp> get HC3AA_temk_1960-1969.mon.gz
```

first time slices to the ones already converted (causing a repetition of data and a confusion about the chronology). Listings of these scripts are given in the Appendix B and C. An example of a typical netCDF header printout using the utility *ncdump* is shown in appendix E (eg. ncdump -h *file name*).

The pressure field from the second OPYC3/LSG run was not available on the IPCC internet site, and was for that reason not converted to netCDF.

The first 10 years from HadCM2 (member 1: HCGS_mslp_1860-1869.mon) could not be read with the code because the ASCII file contained columns that were merged together (eg. -9.990000e+02-9.990000e+02-9.990000e+02-9.990000e+02-9.990000e+02-9.990000e+02-9). These presumably meant missing data, although it was not clear why there should be any missing data in the model results (see Appendix D), but there are some gaps of missing-data according to the IPCC data site. Some of these may be due to problems with archiving the data or lost data. There were also similar gaps of missing-data in members 3 and 4 of the HadCM2 ensemble. These were presumably due to glitches in the archiving of the data.

Table 2 gives an overview of the model results retrieved, converted and evaluated in this study. Appendix F also gives a more detailed model summary from the IPCC site, but there were no available information on the NCAR-DOE nor the GFDL models. There are in total 14 different model integrations (only 13 for SLP).

Although the NCAR CSM (*Boville & Gent*, 1998) data originally were downloaded in the netCDF format from the NCAR CSM internet pages (http://www.cgd.ucar.edu/csm/experiments/b006/), the data were stored as floating point values (4 bytes) and did not use a time axis comparable to the other scenarios (days from the start of integrations as opposed to 'real' dates). A FORTRAN code, *fix_csm.f*, was written to convert to change

Table 3: *AOGCM model scenario overview*

File name	**Model name**	**variables**	**atm. res./lev.**
HC3AA	HadCM3 (Great Britain)	T(1.5m)/SLP	(96x73)/19
HCGS	HadCM2 × 4 (Great Britain)	T(1.5m)/SLP	(96x73)/19
CCGS	CCCma × 3 (Canada)	T(2m)/SLP	T32(96x48)/10
DKGS	2 × ECHAM3/LSG (Germany)	T(2m)/SLP	T42(128x64)/19
MPGS	ECHAM4/OPYC3 (Germany)	T(2m)/SLP	T42(128x64)/19
NCGS	NCAR-DOE (USA)	T(surface air)/SLP	(48x40)
CSGS	CSIRO (Australia)	T(2m)/SLP	R21(64x56)/9
GFGS	GFDL (USA)	T($\sigma_{0.99}$)/SLP	(48x40)
NIGS	CCSR/NIES CGCM (Japan)	T($\sigma_{0.995}$)/SLP	(64x32)
CSM	NCAR CSM (USA) b006	T(surface air)/SLP	T42(128x64)/18

the numerical format from floating point values to scaled 2-byte integers, and thereby reducing the uncompressed file size from 47.2 Mb to 23.6 Mb. The time axis was set to start on 15-January-1990 in order to facilitate easier comparison with the other climate scenarios.

3 Results

3.1 Mean near-surface temperature fields

The converted data were inspected visually as a means of checking that the conversion worked. The visualization of the data was made using NOAA's *Ferret* (*S.Hankin & Denham*, 1994) graphics package. The information on how to read and interpret the ASCII data was difficult to find as this data was given on different web pages not directly accessible from the download page, and sometimes the resulting field was "up-side down" with respect to the north-south axis. The different scenarios were stored with different south-to-north order and there appeared to be no system in the latitudinal order (whereas the CSIRO data was ordered from south-to-north, the HadCM3 (**?**) was ordered from north-to-south), but the later versions of *asc2ncdf.sh* included two options for deciding whether the data were ordered from south-to-north or north-to-south. The inspection of the first attempts to convert the data suggested that the data was "up-side-down" because the Arctic appeared to be colder than the Antarctic and there were mysteriously sharp temperature gradients over open sea. Such gradients tend to be associated with coastal regions. Furthermore, the temperature for the first year in 50°N,0°E was warmest in February-March, whereas in 50°S,0°E it peaked

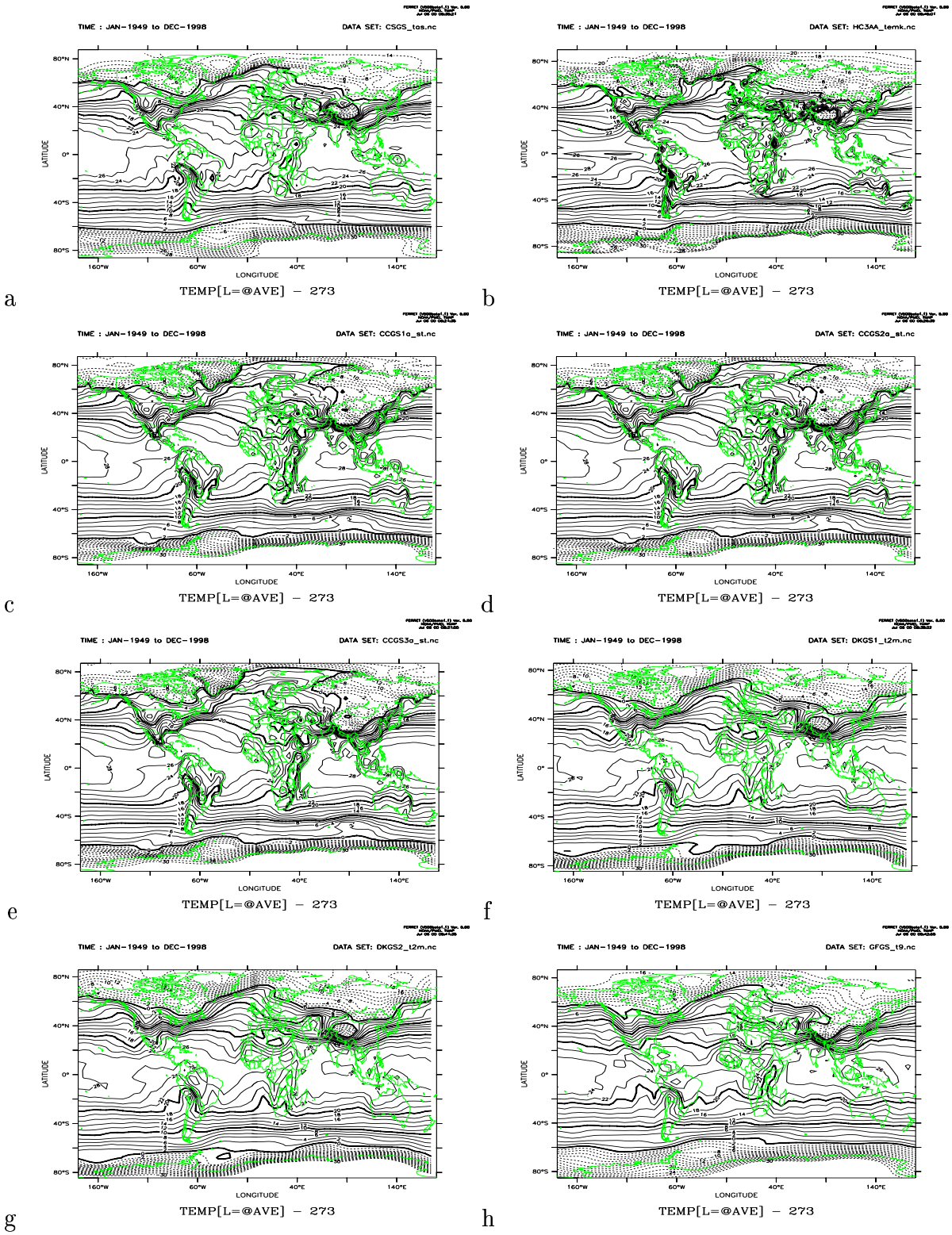

Figure 1: *The mean near-surface temperature (1.5-2m) fields from the converted AOGCM scenarios: a) CSIRO, b) HadCM3, c-f) 3 ensemble runs from CCCma, g) ECHAM3, and h) GFDL.*

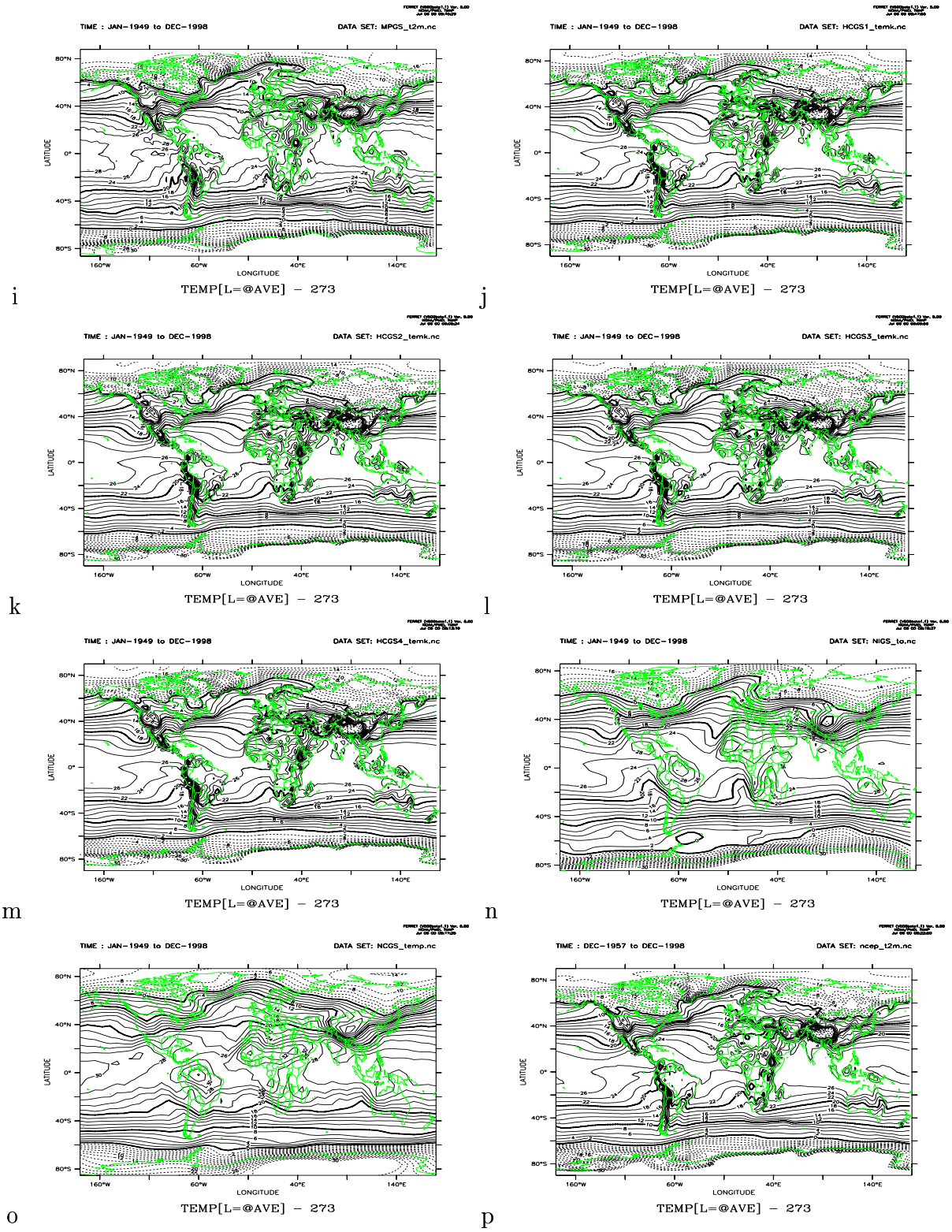

Figure 1: *i-n) The mean near-surface temperature (2m) fields from the converted AOGCM scenarios: i) ECHAM4, j-m) 4 HadCM2 runs, n) CCSR/NIES CGCM, o) NCAR-DOE. p) The mean 2-meter temperature field from NCEP reanalysis II (historical observations).*

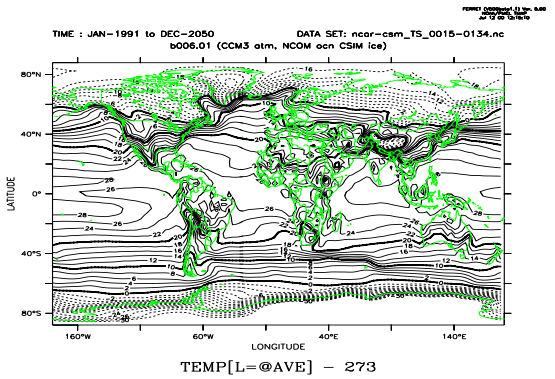

Figure 2: *The mean near-surface temperature field from the NCAR CSM model.*

in June. There was a cold region (below 0°C) in the south Indian Ocean and the warm conditions associated with the North Atlantic drift and the Norwegian current were absent. A code, fix_nc.f, was written to flip the field with respect to latitude.

Figure 1a shows the correct mean 2-meter temperature from the CSIRO (*Gordon & O'Farrell*, 1997) atmosphere-ocean general circulation model (AOGCM), and the warm northeast North Atlantic is in the right place, the cold region is placed correctly over the Himalayas, and the Antarctica is colder than the Arctic. Furthermore, the sharp temperature gradients are aligned up with the coasts. Time plots show (not shown) warmest temperatures in the northern hemisphere during July.

The CSIRO model results (Figure 1a) suggest cold conditions on average (for the 50-year period 1949-1998) over the Himalayas and warm conditions over the Norwegian Sea. The model reproduces a weak "cold tongue" in the upwelling region over the eastern tropical Pacific. This cold tongue region is believed to be important part of the air-sea coupling in the Pacific (ENSO) and is associated with low sea surface temperature (SST). Relatively cold conditions prevail over the mountainous regions in Chile, the Rockies, and high lands in eastern Africa.

The HadCM3 model (**?**) (b) describes a cooler climate than CSIRO over northern Scandinavia, Siberia, and northern Canada. The reproduction of the cold tongue in the eastern equatorial Pacific is too prominent, as it is much stronger than the other models and the NCEP reanalysis. This model did not use flux correction, and similar discrepancies in the other models may have been reduced by such adjustments ("fudging"). The Andes, the Rockies and Kilimanjaro mountain climates are more realistic in the HadCM3

simulation (see the observed analysis in panel p).

The three CCCma T(2m) simulations (*McFarlane* et al., 1992; *Boer* et al., 1998a,b) are shown in Figure 5c-e, and these are similar to each other. They are warmer over the Arctic than both CSIRO and HadCM3, but give a cooler climate over eastern Africa and Mongolia.

The two T(2m) results from ECHAM3 (DKRZ reports No.6 and No.2, 1998) (f,g) suggest colder conditions than CSIRO and CCCma over northern Scandinavia, and are in this respect similar to HadCM3. But they also suggest a colder Labrador Sea than the HadCM3 model.

The mean GFDL model surface air temperature (h) is similar to that of CSIRO, but this model has a weaker cold tongue in the eastern tropical Pacific and parts of Mongolia is colder. The east African high land is also colder in the GFDL model than in the CSIRO, HadCM3, and ECHAM3 models.

The ECHAM4 simulation (i) is similar to that of HadCM3, but with warmer conditions over the Barents Sea area and a much less pronounced cold tongue in the eastern tropical Pacific. The southern coast of Brazil is warmer in the ECHAM4 model than in the HadCM3 scenario.

The four HadCM2 (*Cullen*, 1993) integrations (j-m) show similar features, with similarities to ECHAM4 over northern Scandinavia, but warmer than the HadCM3 scenario.

The CCSR/NIES CGCM (*Emori* et al., 1999) (n) results is similar to those of ECHAM3, but gives much warmer conditions over northern Brazil, Chile, and the Himalayas. This model gives a less realistic description of the climate in the mountain regions than the other models.

The historical analysis of the 2-meter temperature from NCEP re-analysis (eg see *Benestad* (1999b) for more details) is shown in Figure 1p. A comparison with the model simulations suggests that the CCCma, NCAR-DOE generally give a too warm climate, and that the HadCM3 predicts warmer conditions over extensive parts of the Indian Ocean, Indonesia and the western Pacific.

Because the NCAR CSM (*Boville & Gent*, 1998) integration did not use historical forcing, but the present day CO_2 level (355ppm) for the first 10 years and then a 1% increase thereafter, the results from this model cannot be compared directly with the other scenarios. The mean surface temperature field for the 1991-2040 period is nevertheless shown in Figure 2, and although this plot shows a projection of the future climate, it has similar character to the historical mean temperature field, although with higher temperature in the eastern tropical Pacific. The NCAR CSM model also predicts colder conditions for Scandinavia, despite the projected global warming.

3.2 Mean near-surface temperature evolution over Norway

The estimated (area weighted) global mean temperatures from the various IPCC scenarios shown in Figure 3 differ in terms of the 1990's temperature levels, most probably due to different spin-up strategies and initial conditions, but also possibly due to different model formulations. The HadCM3 model is integrated with no flux correction. The NCAR-DOE model (thick green) suggests a significantly warmer global climate than the other models. The GFDL model (blue) is substantially cooler than the other models.

Regional mean temperature curves for Norway, the Norwegian Sea and the Barents Sea are shown in panels b, c, and d of Figure 3. These curves indicate stronger fluctuations than the global mean temperature estimates. The mean temperature from HadCM3 over the Scandinavian region (58°N-70°N, 5°E-30°E) in panel b is lower than in the scenarios, but the NCAR-DOE model indicates the warmest conditions over Scandinavia. The members within the respective CCCma and HadCM2 ensembles follow each other closely.

There are apparent periods with cooling or stable conditions, such as after the 1970s in the HadCM3 results. There are similar brief cooling events in the other scenarios as well. One may ask whether these events are due to changes in the ocean circulation (the heat poleward transport from the subtropical Atlantic gyre into the Norwegian Sea, or changes in the oceanic meridional overturning: a "thermohaline catastrophe"), however, there is insufficient data to answer this question here. The NCAR-DOE model indicates a distinct upward jump in the temperature after 1990.

The NCAR CSM curves (thick blue) indicate colder climatic conditions than the other models over the Nordic countries, but the global mean temperature is similar to the other scenarios. The global mean temperature trend is the lowest of the 15 scenarios, but the warming in the Norwegian Sea region (fig:gmtc) is among strongest of the model scenarios.

There appears to be more variability in the HadCM3 and NCAR-DOE results than the others, which is also evident in the 30-year running variance plots in Figure 4. Whereas the results in Figure 3 exhibit the interannual variations, Figure 4 shows all variance with time scales between 1-360 months. Thus, the annual cycle is a prominent feature of the results in Figure 4.

The Japanese CCSR/NIES model (Figure 4a, cyan) describes significantly stronger temperature variations over Scandinavia than the other AOGCMs. All models indicate a reduction in the temperature variance, probably due to a reduction in the amplitude of the annual cycle (eg warmer winters). Apart from the CCSR/NIES results, the HadCM3 and NCAR-DOE model results are associated with the highest level of variance over Scandinavia. The

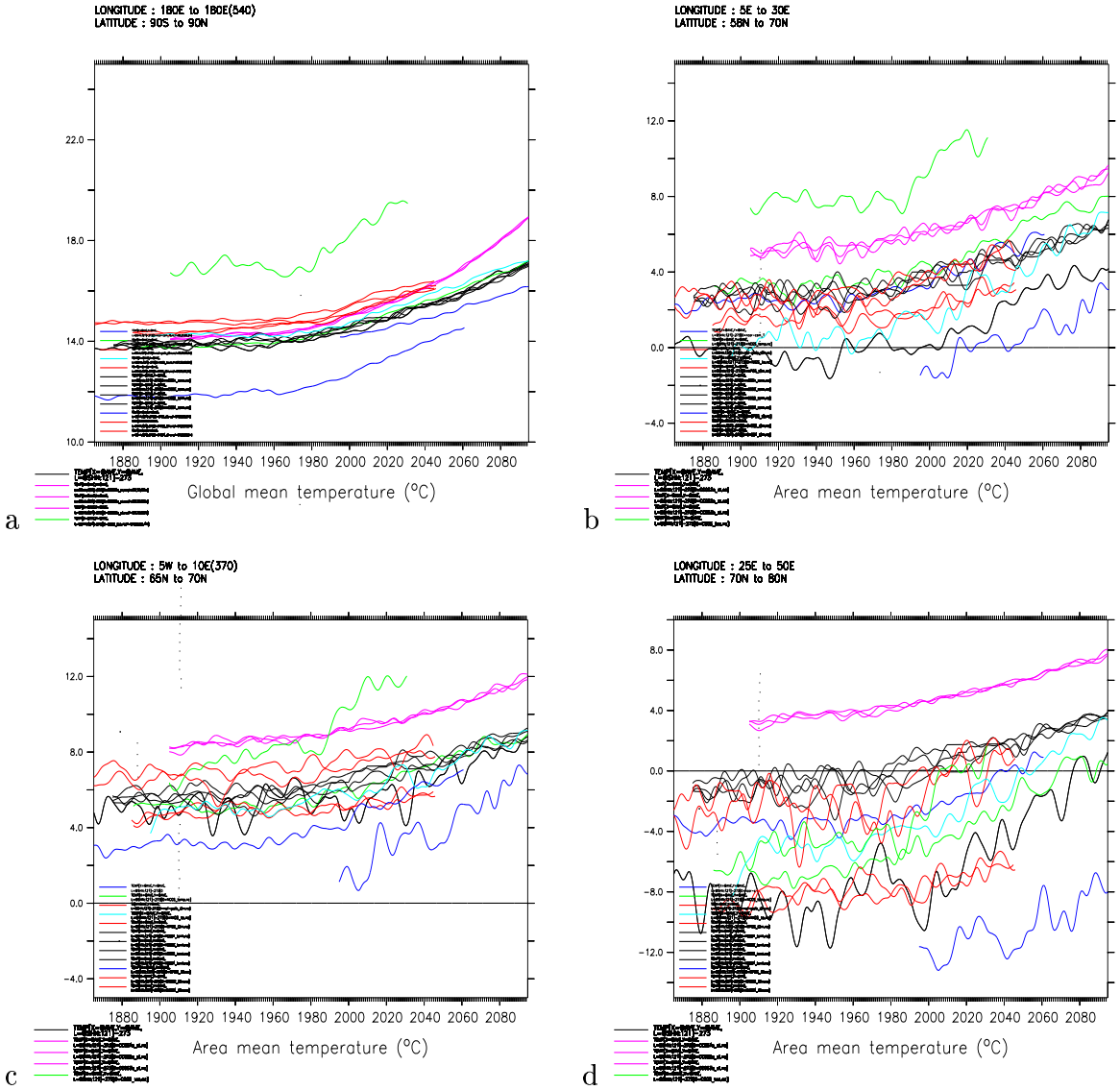

Figure 3: *a) Estimated global mean temperature for the different scenarios: The heavy black line represents the HadCM3 results, thin black the 4 members of HadCM2, the magenta lines are the 3 Canadian ensembles, the thin green represents the CSIRO results, cyan CCSR/NIES , the red lines ECHAM3 (thin) ECHAM4 GSDO (bold) and GSDIO (extra bold), thin blue the GFDL model, and heavy blue the NCAR CSM model. b) The area mean temperature for the Nordic region, c) the Norwegian Sea region, and d) the Barents Sea region. The temperatures were low-pass filtered using a 121-month Hanning filter.*

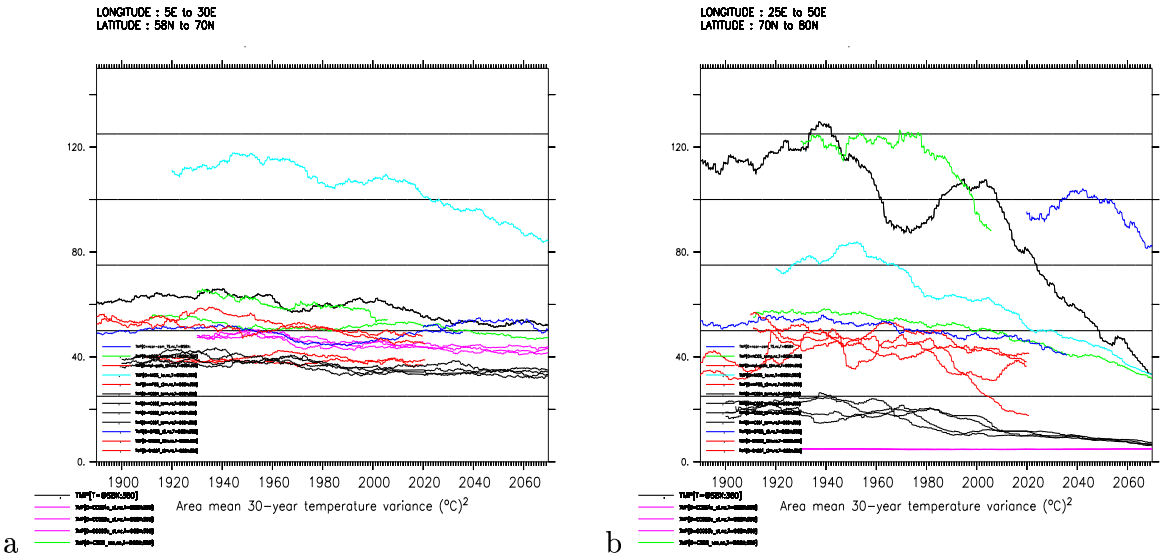

Figure 4: *a) Estimated running 30-year temperature variance over the Nordic region for the different scenarios: The heavy black line represents the HadCM3 results, thin black the 4 members of HadCM2, the magenta lines are the 3 Canadian ensembles, the thin green represents the CSIRO results, the thick green the NCAR-DOE model, the red lines ECHAM3 (thin) ECHAM4 GSDO (bold) and GSDIO (extra bold), CCSR/NIES (cyan), thin blue the GFDL model, and heavy blue the NCAR CSM model. b) Same as in a), but for the Barents Sea region.*

ECHAM3 and HadCM2 integrations indicated the lowest levels of variability over Scandinavia.

For the Barents Sea region (Figure 4b), the HadCM3 (black) and both the NCAR-DOE models (green and thick blue) show substantially higher levels of variance than the other models. All the models suggest a future decrease in the temperature variance over this region. By 2060, the HadCM3 variance level is predicted to drop to similar levels as given by the GFDL and the CSIRO AOGCMs. All the CCCma integrations predict very low levels of variance over the Barents Sea.

All scenarios suggest low-frequency fluctuations in the temperature variance level, and this is most clearly seen in the HadCM3 results over the Barents Sea, indicating a rapid drop after 1940, and then an increase between 1980 and 2000. There are only marginal variations in the Barents Sea temperature variance level in the CCCma results.

3.3 Mean SLP fields

All the models except for the GFDL describe mean low-pressure conditions over Iceland and the Aleutian islands and high-pressure over the Azores, subtropical Pacific off the Californian coast, in south Atlantic, south Indian ocean, and southeastern Pacific. All models, except for the GFDL and CCSR/NIES CGCM produce strong and zonally symmetric meridional SLP gradients (strong zonal geostrophic winds) between 40°S and 60°S. The strength and extent of the various pressure systems vary among the different models.

The GFDL model (g) describes few semi-permanent high- or low-pressure systems over the oceans, but places these instead over the continents. This is different to the historical observations (o), and it is therefore likely that this model is unsuitable for making future climate scenarios.

The CCSR/NIES CGCM (m) produces semi-permanent pressure systems somewhat similar to the other models, but the meridional SLP gradient in the southern is not symmetric. The band of strong zonal geostrophic winds is also displaced poleward over the Antarctica.

The mean SLP field from the NCAR CSM is shown in Figure 6a, and despite the fact that these results represent a future climate scenario, the main features are similar to those of the historical observations and the AOGCM reproduction of the past climate.

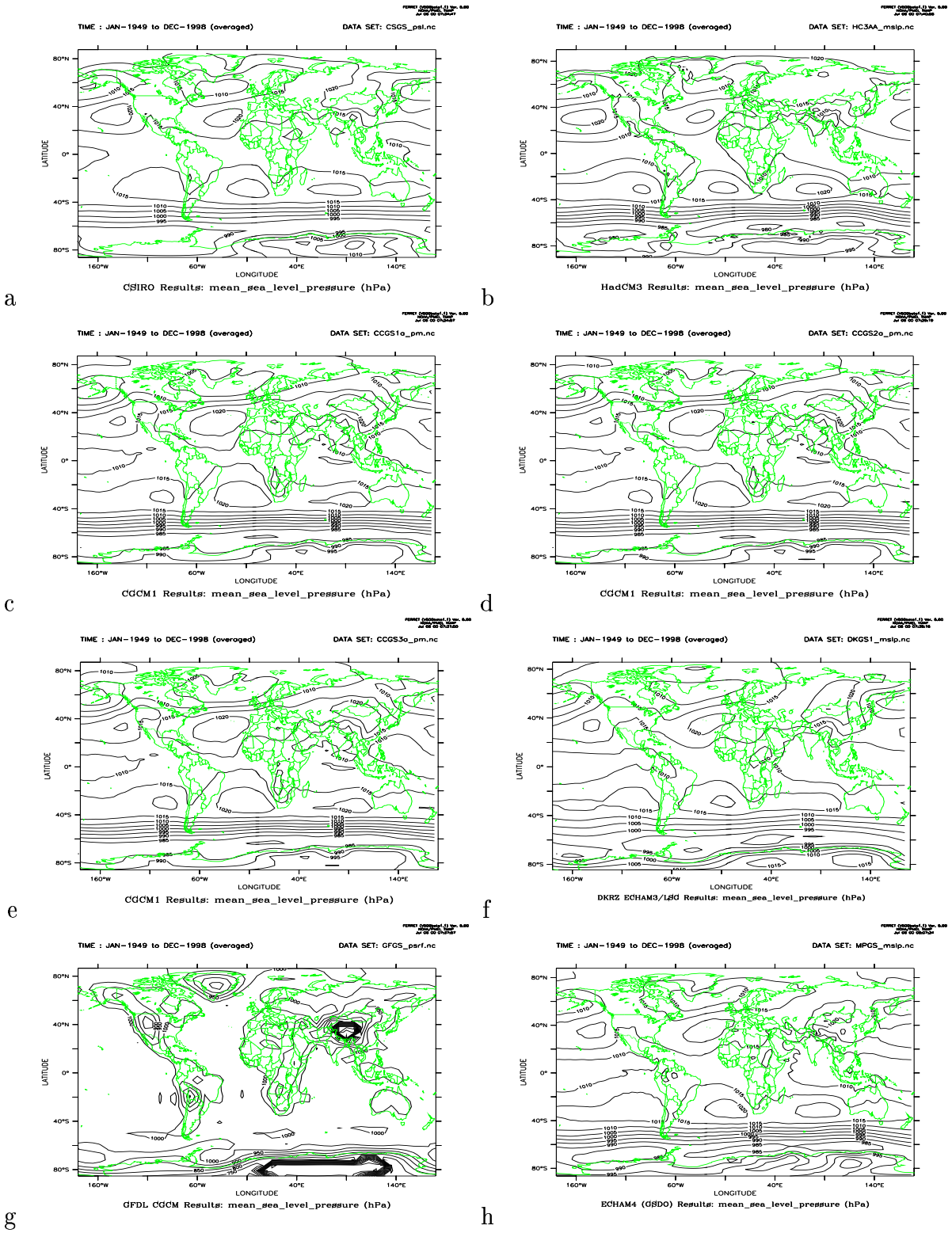

Figure 5: *The mean SLP fields from the converted AOGCM scenarios.*

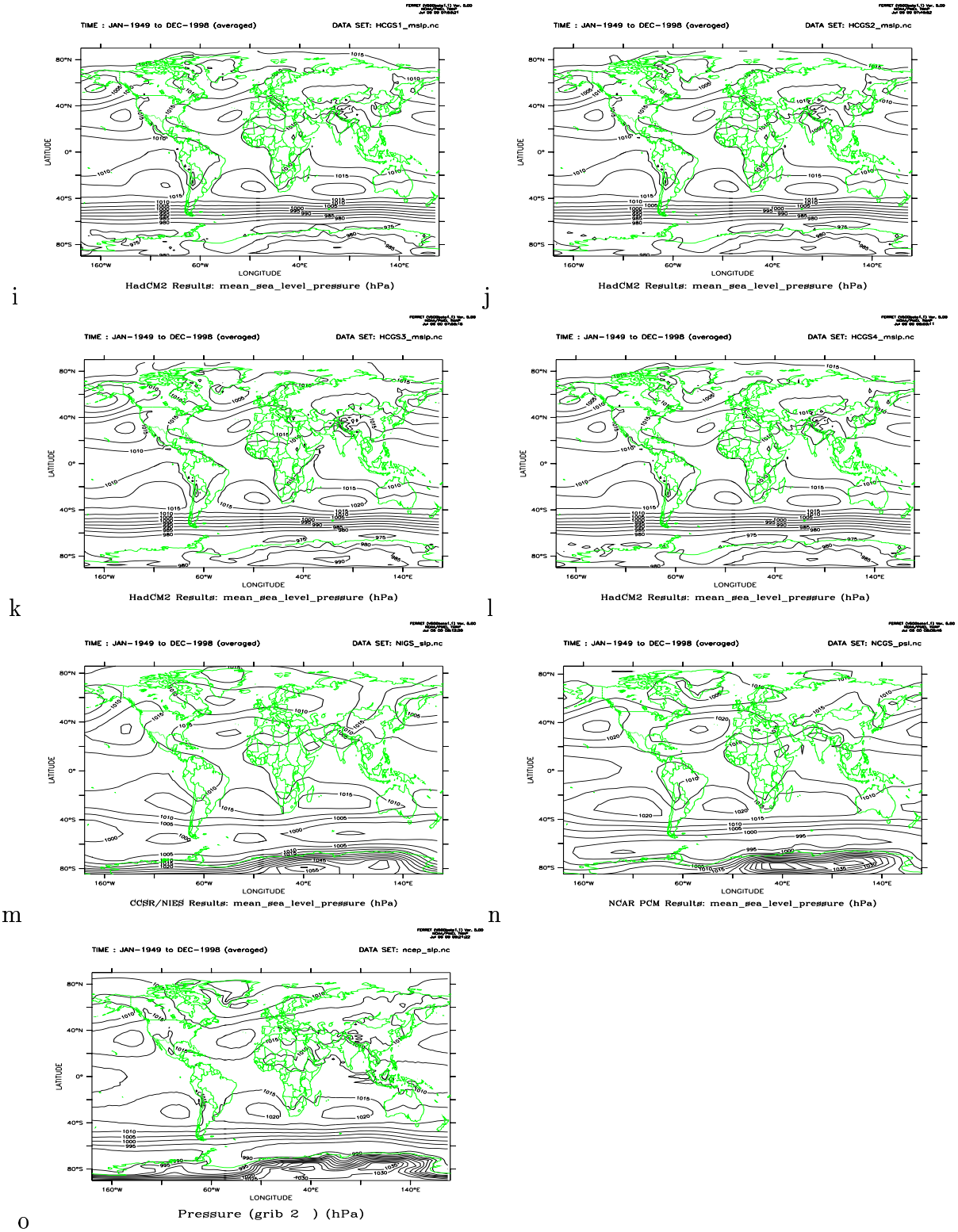

Figure 5: *i-n) The mean SLP fields from the converted AOGCM scenarios. o) Corresponding analysis from NCEP reanalysis II.*

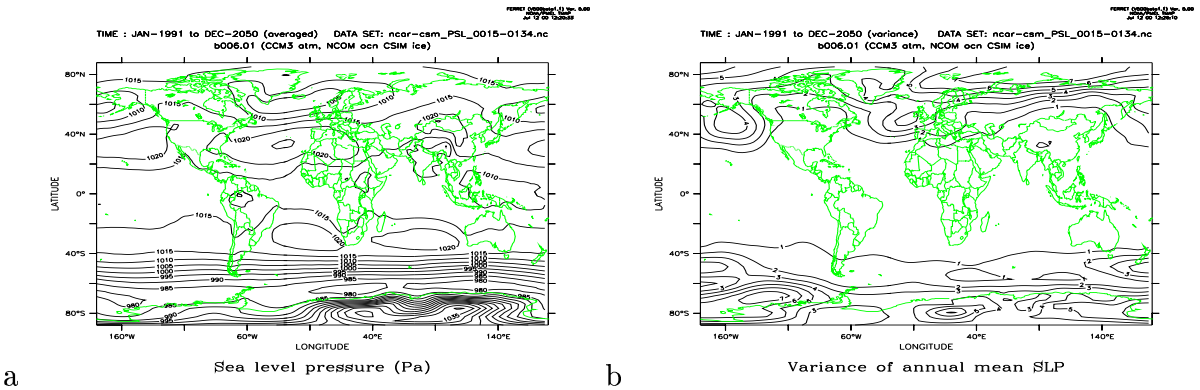

a b

Figure 6: *The mean SLP field (a) and SLP variance (b) from the NCAR CSM model.*

3.4 Annual mean SLP variance

Another quantity to look for is the spatial distribution of variance the annual mean SLP. Most of the climate models produce high variance in the vicinity of Greenland and Iceland, over the Aleutian islands/north Pacific, and Antarctica (the low-pressure regions).

The CSIRO model (Figure 7a) may produce too weak annual mean SLP fluctuations over Antarctica. This discrepancy is common for all the model simulations, assuming that the NCEP reanalysis gives a true description of the SLP in this region[1]. The HadCM3 gives stronger annual mean SLP fluctuations over the north Pacific.

The CCCma model (c-f) describes smaller variance over the Aleutian islands than the model consensus. There are some differences between the ensemble members in the polar regions, which may be taken as being due to the analysis uncertainty or noise.

The ECHAM3 scenario (f) is similar to the CSIRO variance field, but with substantially stronger annual SLP variance over eastern Greenland and over the Himalayas.

The GFDL model (g) fails to reproduce the high annual mean variability over the Antarctica, and the contours are characterized by the low model resolution.

The ECHAM4 model (h) scenario is similar to the HadCM3, but with stronger fluctuations near the Himalayas.

The four HadCM2 scenarios (i-l) are again similar, but also resemble the results from ECHAM4, with the exception of the Himalayas region. The

[1]There may be problems with the NCEP SLP over the Antarctica, due to the sparseness of the observations and the closeness to the pole.

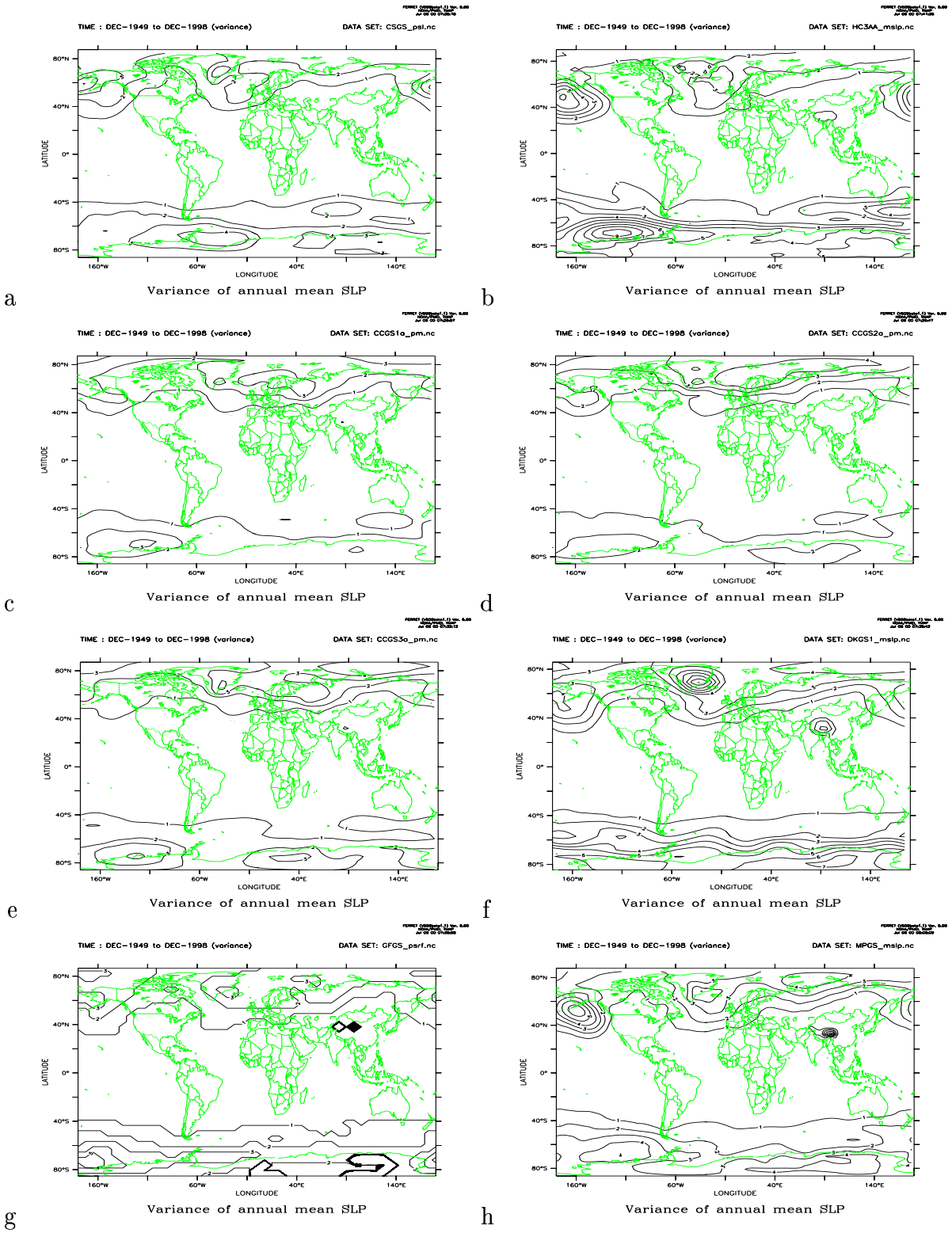

Figure 7: *The SLP variance fields from the converted AOGCM scenarios.*

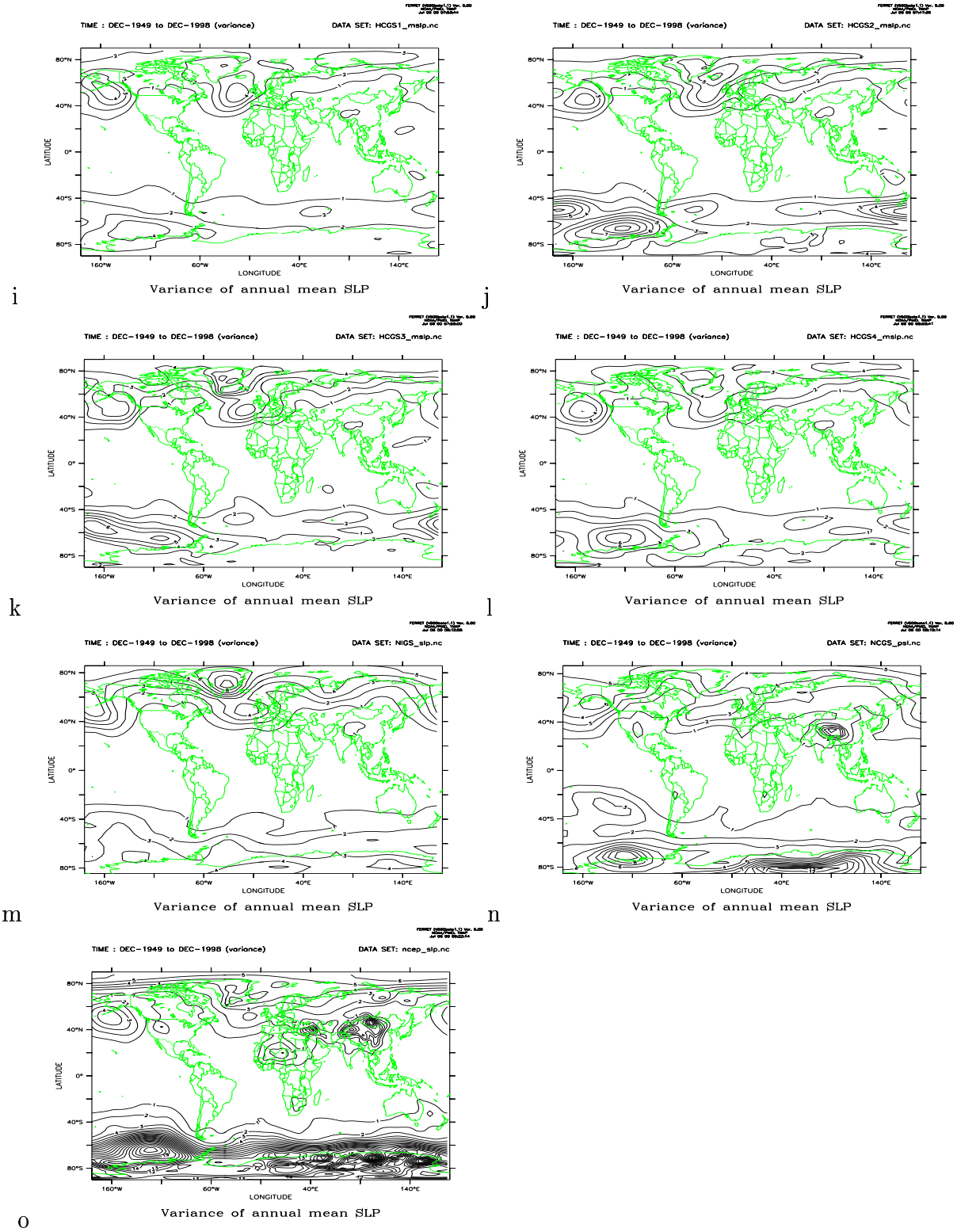

Figure 7: *i-n) The annual mean SLP variance fields from the converted AOGCM scenarios. o) Corresponding field from NCEP reanalysis II.*

differences between the ensemble members can be interpreted as a measure of the robustness of the variance analysis, and two of the members (j,k) indicate stronger SLP variance over eastern Greenland than the others (i,l). It is therefore difficult to say whether the HadCM2 model produces stronger annual mean SLP fluctuations over Greenland than the HadCM3 model.

The CCSR/NIES CGCM (m) results are similar to the CSIRO results, but with stronger variance over Greenland and the North Atlantic.

The variance field of the NCAR-DOE model (n) indicate high levels near the North Atlantic storm track and the Himalayas. This model also produces higher levels over the Antarctica.

The annual mean SLP variance field of the NCEP reanalysis II is shown in Figure 7o. The historical analysis suggest much stronger variance in the annual mean SLP over the Antarctica, but more similar features in the northern hemisphere. One important detail may the region of high variability stretching from Iceland to Svalbard, not seen in the model scenarios. The observations also suggest higher annual mean SLP variance levels over the Sahara region, the middle east, the Himalayas, and Mongolia.

Figure 6b shows the annual mean SLP variance field for the NCAR CSM results, which has a similar character to the corresponding results in the HadCM3 (Figure 7b), even though these are not directly comparable.

3.5 The North Atlantic Oscillation index

Local climate variations in parts of Norway are strongly influenced by the large-scale SLP structure associated with the North Atlantic Oscillation (NAO) (*Kapala* et al., 1998; *Benestad*, 2001, 1998). Therefore, the model description of the NAO is important for climate studies for northern Europe. The NAO conditions are often described in terms of the North Atlantic Oscillation Index (NAOI) (*Jones* et al., 1997), often taken as the normalized SLP difference between Lisbon and Iceland. The NAOI was estimated similarly for all model results, by the means of bilinear interpolation.

Figure 8 shows estimates of the NAOI for the various model runs. It is evident from this plot that the NAO has a noisy appearance and according to the model consensus, it is not related to the global warming in any systematic way. However, the ECHAM4 model has a tendency to favour a systematic strengthening whereas the HadCM2 models indicate a weakening of the NAO. The NCAR CSM (thick blue) shows a slight strengthening of the NAO, as seen in the ECHAM4 scenario (thick red).

Gaps of missing data can be seen in the NAO index (NAOI) of HadCM2 members 3 and 4. These gaps were due to similar problems as mentioned in 2, due to missing data in the original ASCII files (Appendix D).

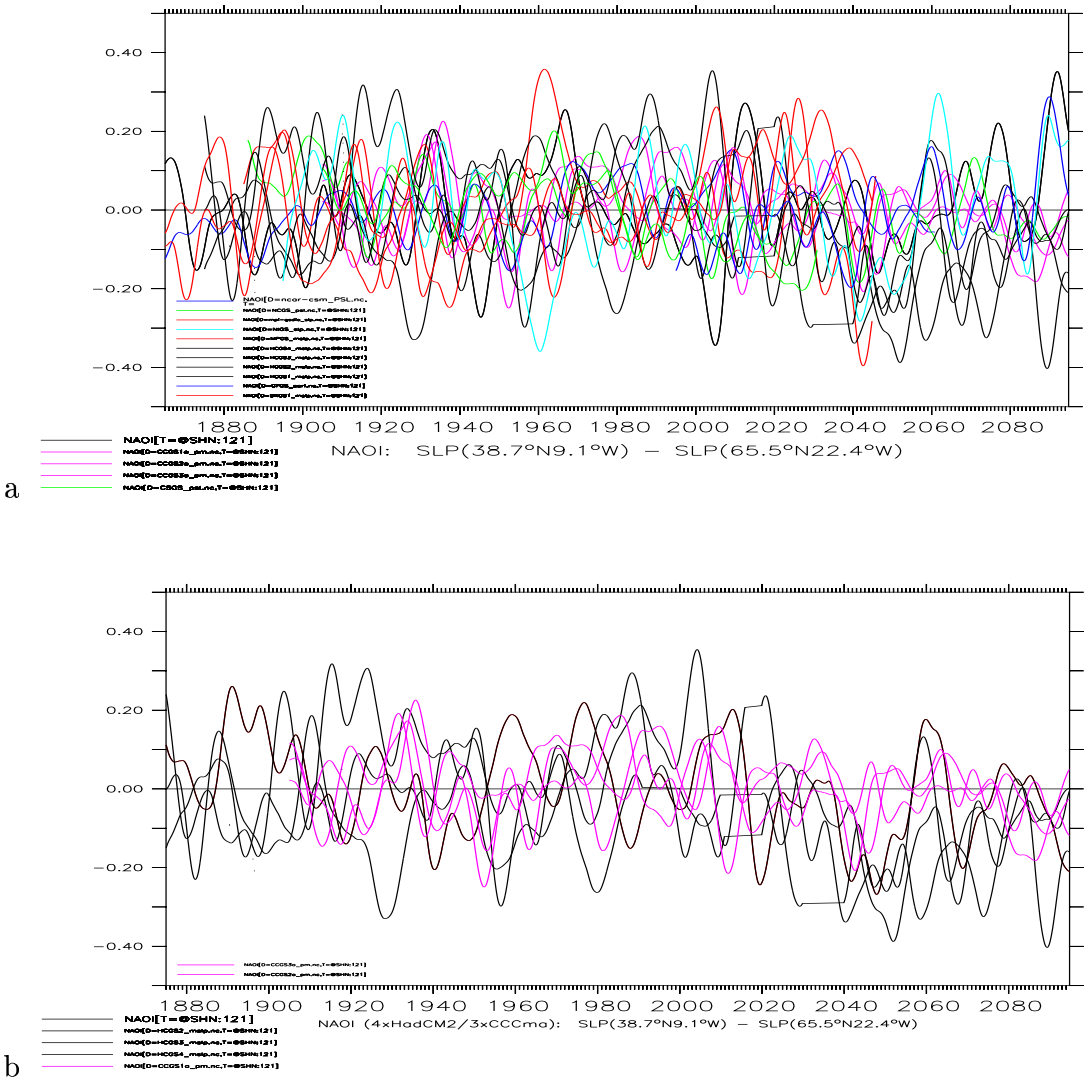

Figure 8: *a) Estimated NAOI for the different scenarios: The heavy black line represents the HadCM3 results, thin black the 4 members of HadCM2, the magenta lines are the 3 Canadian ensembles, the thin green represents the CSIRO results, the red lines ECHAM3 (thin) ECHAM4 GSDO (bold) and GSDIO (extra bold), cyan CCSR/NIES, thin blue the GFDL model, and heavy blue the NCAR CSM model. b) The same as a), but showing just the HadCM2/CCCma ensembles.*

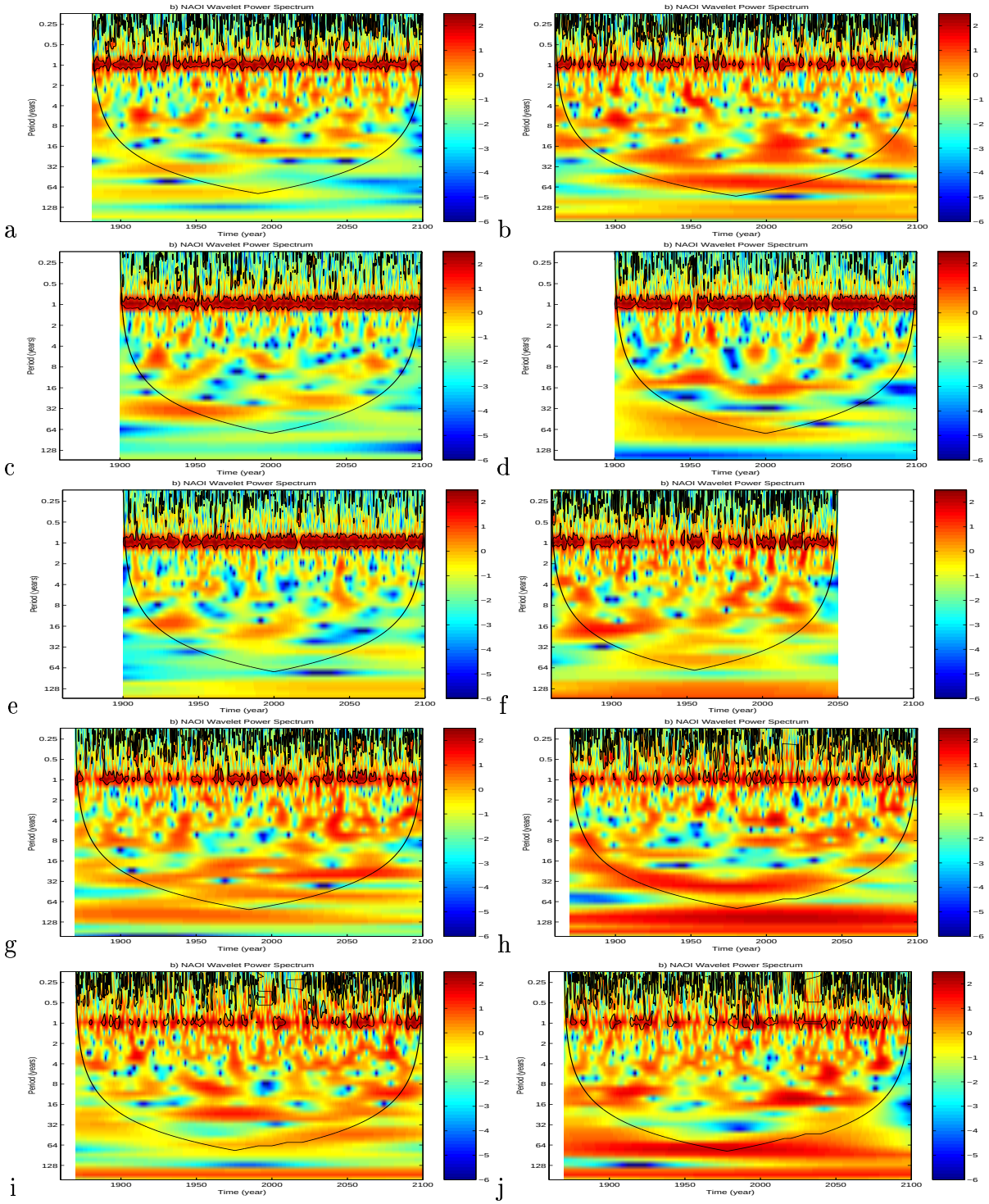

Figure 9: *The wavelet spectra of the NAOI from CSGS (a), HadCM3 (b), CCGS1-3 (c-e), ECHAM4 (f), and HadCM2 (g-j).*

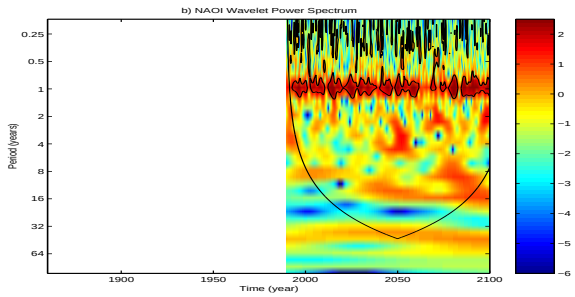

Figure 10: *The wavelet spectra of the NAOI from the NCAR CSM scenario.*

The various HadCM2 members show completely different short-term behaviour in the NAO, suggesting that this is related to non-linear chaotic processes. But, there all the ensemble members suggest a long-term weakening of the NAO for the future. Hence, in the HadCM2 the NAO seems to affected the external forcing or the global climate state, in addition to being chaotic. The members from the Canadian ensemble also give different NAOI developments within the ensemble, however, these suggest no systematic changes to the NAO character. These results may be interpreted as the NAO in the CCCma being completely chaotic and not influenced much by the general climate conditions nor by the external forcing.

Figure 9 shows the wavelet spectra of the NAOI from a number of model results. The NAOI was estimated for all seasons, and the annual cycle shows up as a prominent band of high variance at 12 month cycles. Only variability with yearly and time scales shorter than one year show up as statistically significant due to the noisy character of the NAOI. There are significant variations in the NAO seasonal cycle in most of the model results. Some of the breaks in the high frequency variability seen in the HadCM2 results are due to gaps of missing data (see section 2).

There are some changes in the low-frequency variability, although not statistically significant in the unfiltered all-season time series. These results indicate that the decadal time scales are not robust, but may vary from time to time. The strength of the annual cycle in the NAOI varies with time.

The NAOI from the HadCM3 (b) gives a hint of a strengthening the multi-decadal (τ=8-16 years) variance after 1900 as well as a modulation in the decadal band (τ=32-64 years), but these results may not be robust. There are also suggestions of a weakening of 40-50 year fluctuations towards the end of the scenario, but changes are by no means statistically significant.

The second member of HadCM2 model (panel h) suggests stronger low-frequency (mulitdecadal and centennial) changes than the other models, but members 3 and 4 from HadCM2 (i and j), ECHAM4 (f), and CCGS3 (e) also

suggest some long-term changes in the NAOI. The finding that the NAOI in one of HadCM2 and two of the three CCCma members were associated with much less long-term variance than the rest of their ensemble members, may point to a non-linear chaotic NAO process, even for low frequencies. The annual cycle in the NAO in the HadCM2 ensemble is less pronounced than in the CCCma runs.

The NCAR CSM scenario for the NAO may suggest an intensification in the decadal frequency band (Figure 9), however, these variations do not qualify as statistically significant in the wavelet analysis.

On the whole, there are no systematic change in the NAOI character according to the model consensus, such as seen in the area mean temperature variance level over Scandinavia or the Barents Sea in section 3.2.

3.6 The Southern Oscillation indices

The El Niño Southern Oscillation (ENSO) is one of the most important modes of natural variability, after the diurnal and annual cycles. ENSO affects weather and climate over large parts of the world. The state of ENSO can be represented by the Southern Oscillation Index (SOI), which is the normalized pressure difference between Darwin and Tahiti. The SOI was estimated similarly for all model results, by the means of bilinear interpolation.

Figure 11a shows estimates of the Southern Oscillation index for the various models. Again, there is no clear consensus among the various models as to what to expect about ENSO for the next 50 years. But within each ensemble, the respective models tend to give a similar long-term projection for ENSO. The Canadian model (CCCma, magenta curves), also shown in Figure 11b, indicate a systematic increase in the SOI, or a tendency towards more La Niña type conditions. The HadCM2 ensemble indicates no systematic change in the character of ENSO. This is in agreement with *Collins* (2000) before the greenhouse gas concentrations reach 4 times the pre-industrial levels.

In contrast to the NAO, for which the CCCma indicated no systematic long-term changes, all the CCCma members predict a clear positive trend in the SOI, and this trend starts at the beginning of the integration which is 1900. In comparison, there has been no such trend in the SOI from the real world, implying that CCCma's "historical reproduction" of the SOI is associated with systematic errors. The HadCM2 results, which indicated a weakening of the NAO, on the other hand, suggest no systematic long-term changes to the SOI.

These results suggest that the long-term evolution of ENSO in the models to a large extent depends on differing details in model description of the

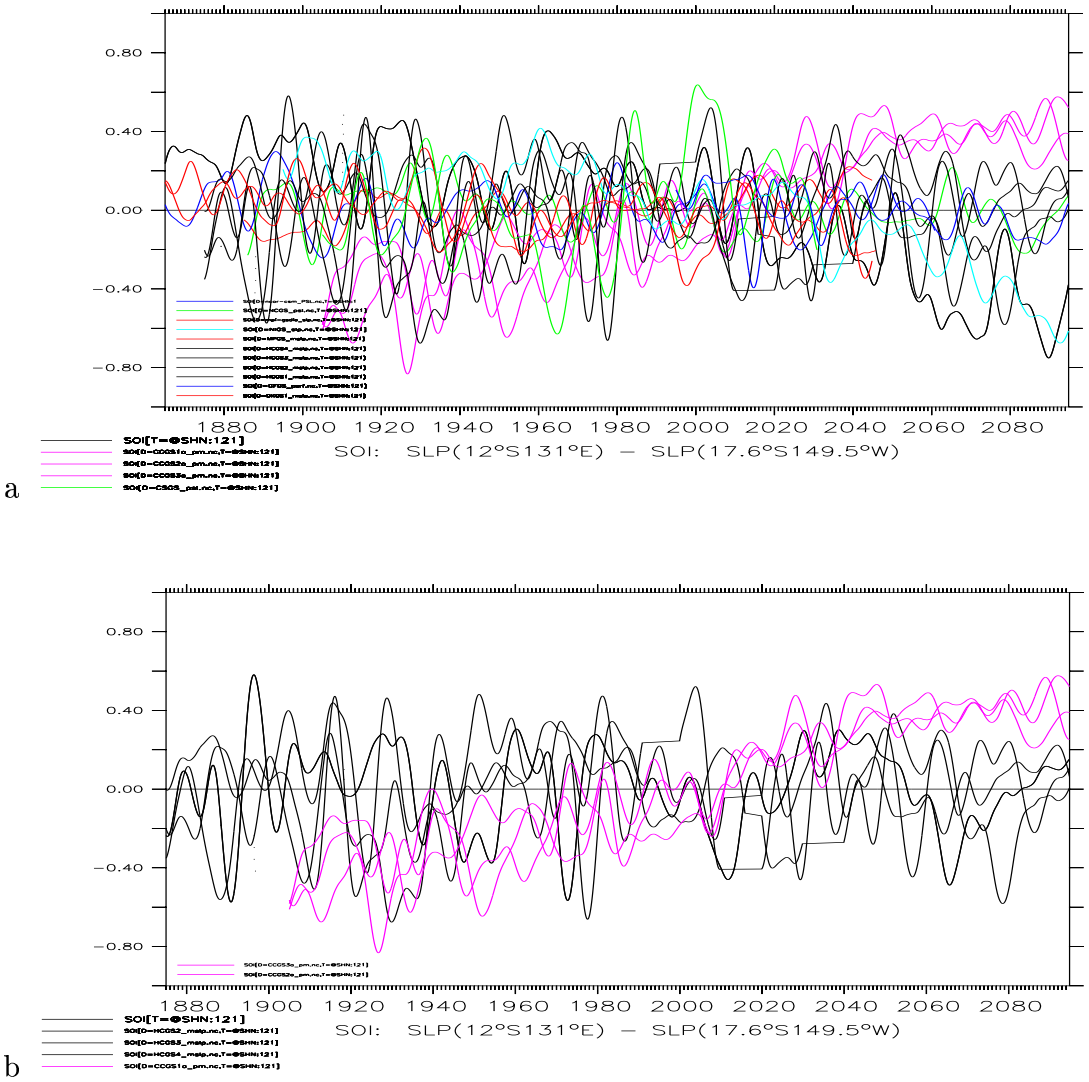

Figure 11: *a) Estimated SOI for the different scenarios: The heavy black line represents the HadCM3 results, thin black the 4 members of HadCM2, the magenta lines are the 3 Canadian ensembles, the thin green represents the CSIRO results, the red lines ECHAM3 (thin) ECHAM4 GSDO (bold) and GSDIO (extra bold), cyan CCSR/NIES , and blue the GFDL model. b) The same as a), but showing just the HadCM2/CCCma ensembles.*

climate system. The HadCM3 indicates a substantial strengthening of El Niño conditions (negative trend in SOI) and the ECHAM4 model make projections of a slight bias towards stronger El Niño. The ECHAM3 model, on the other hand, predicts a slight positive trend in the SOI.

3.7 The coupling between near-surface temperatures and SLP

In order to evaluate the models' skill of describing the air-sea coupling processes, a canonical correlation analysis (CCA) was applied to the model SLP and near-surface temperature. The leading SLP-T(surface air) CCA patterns are strongly influenced by the NAO, and it is crucial that the AOGCMs reproduce the SLP-T(surface air) relationship if there is a robust relationship between these two quantities in the real world. These CCA results may be used to point out those models which are not suitable for the study of climate change in the North Atlantic and Nordic Seas region.

The polarity of the anomalies in Figure 12 is arbitrary, but it is important that the polarity of the SLP pattern corresponds to the correct polarity of the temperature. In other words, a strengthened NAO SLP condition must correspond to a strong NAO temperature pattern, and a weak NAO SLP anomaly corresponds to a weak NAO temperature response.

The leading pair of CCA patterns in the HadCM3 model results is shown in the panels a and b, bearing a strong resemblance to the NAO with a north-south SLP dipole with centres of action over Iceland and the Azores and anti-correlated temperatures over Greenland and northern Europe. The strongest temperature weights are seen over western Norway, in contrast to over the Baltics in the historical analyses (Figure 12β, γ, *Note that the observations are shown for a larger region than the model results*). It is important to note that these results are not directly comparable to the historical observations, as the CCA was applied to the entire HadCM3 scenario, and the differences may be due to different lengths of the periods analysed, the future climate developments, or sampling fluctuations. The large-scale features of the coupling between the near-surface thermodynamical-dynamical processes (advection) are nevertheless realistic.

The corresponding analysis for the HadCM2 results are shown in panels b-j. A strengthened NAO condition is associated with warm anomalies in the Nordic countries and low temperatures in Greenland and over Labrador, and vice versa. The strongest weighting in temperature is found in southern Scandinavia and the interior of Greenland. A second European temperature maximum is seen over the Baltics, more in agreement with the historical

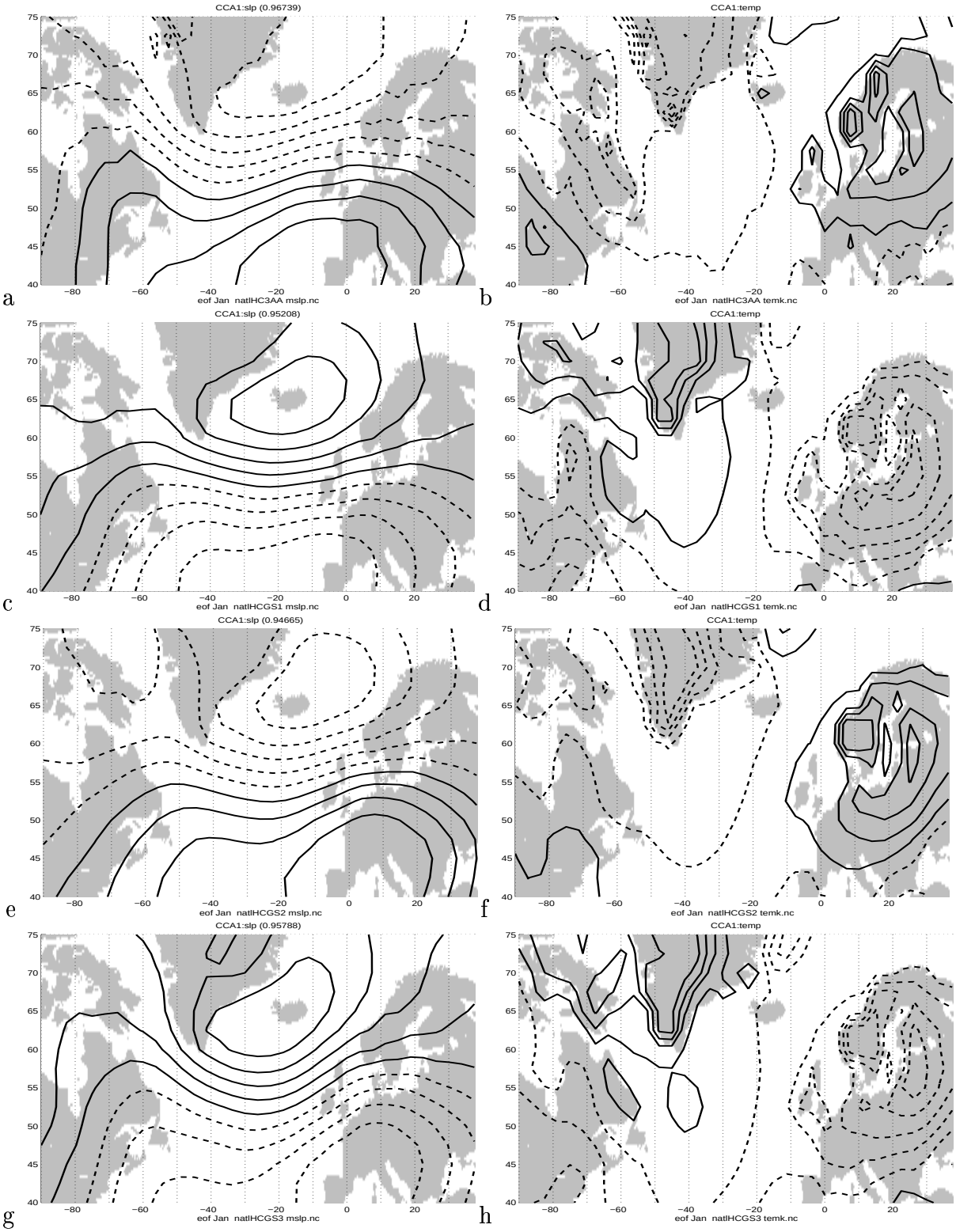

Figure 12: *The leading CCA SLP-Temperature patterns in various AOGCM results. Left: SLP, Right: near-surface temperature. The results are for HadCM3 (a,b) and HadCM2(c-h).*

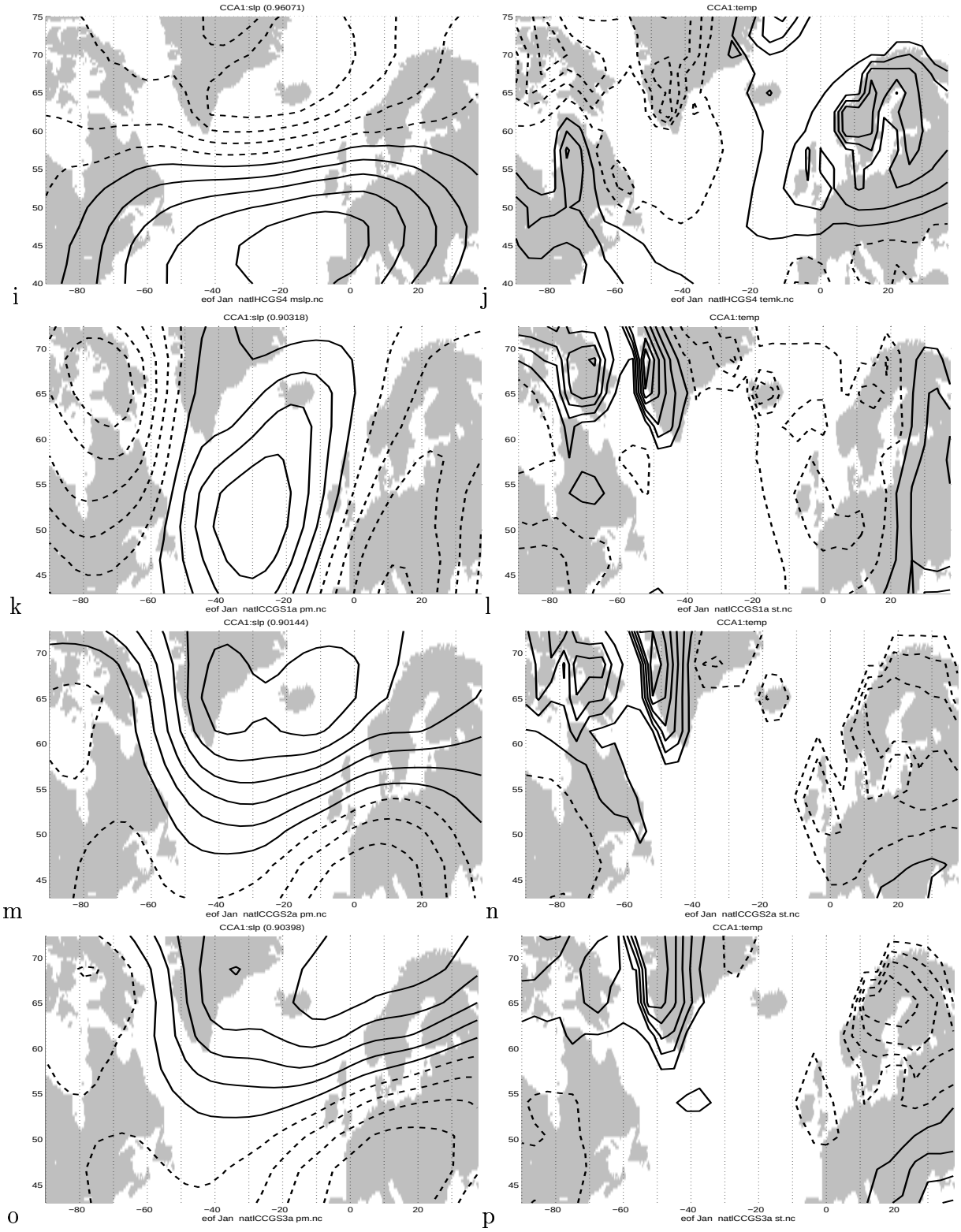

Figure 12: *The leading CCA SLP-Temperature patterns in various AOGCM results. Left: SLP, Right: near-surface temperature. The results are for HadCM2(i,j) and CCCma (k-p).*

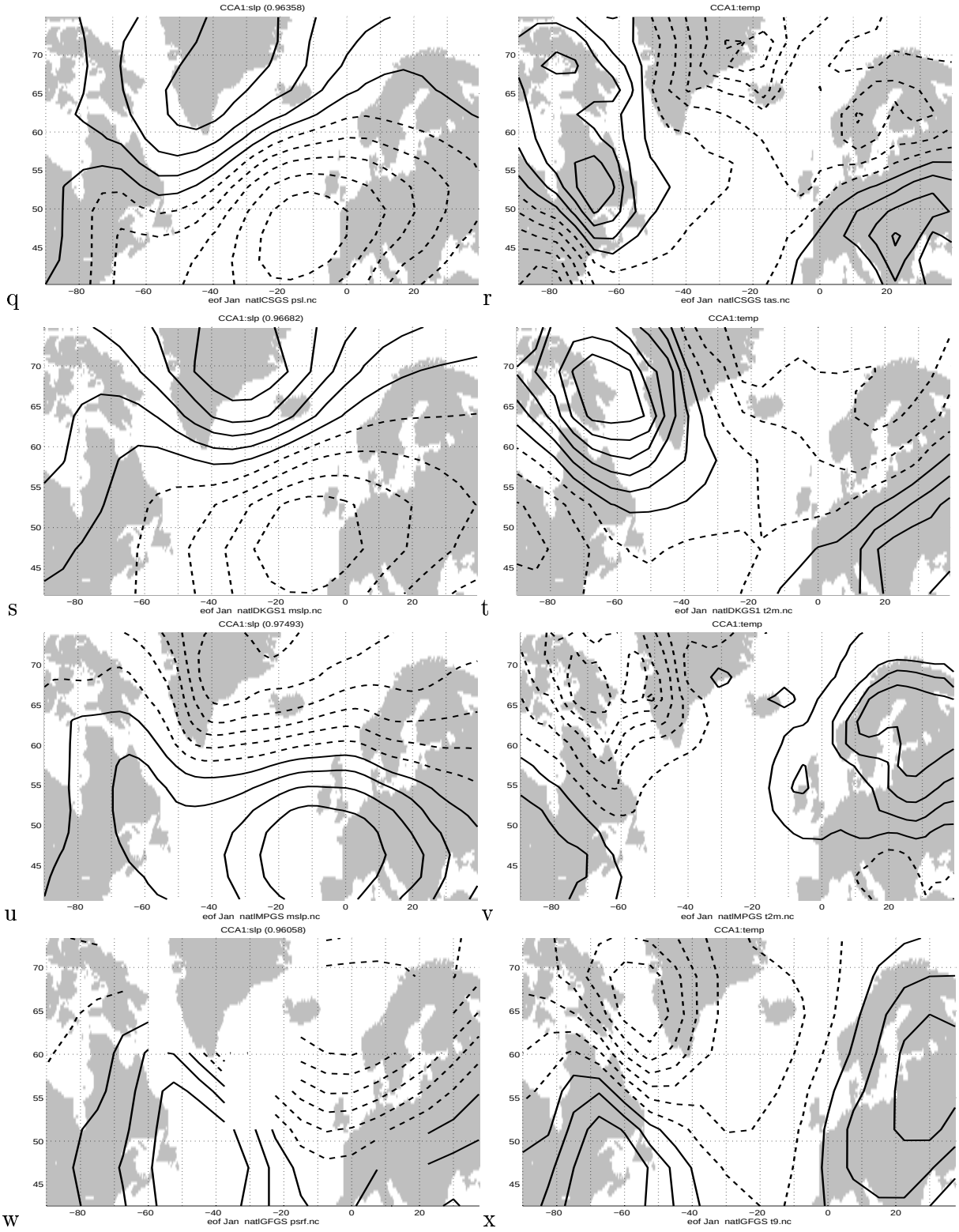

Figure 12: *The leading CCA SLP-Temperature patterns in various AOGCM results. Left: SLP, Right: near-surface temperature. The results are for CSIRO (q,r), ECHAM3 (s,t), ECHAM4 (u,v) and GFDL (w,x).*

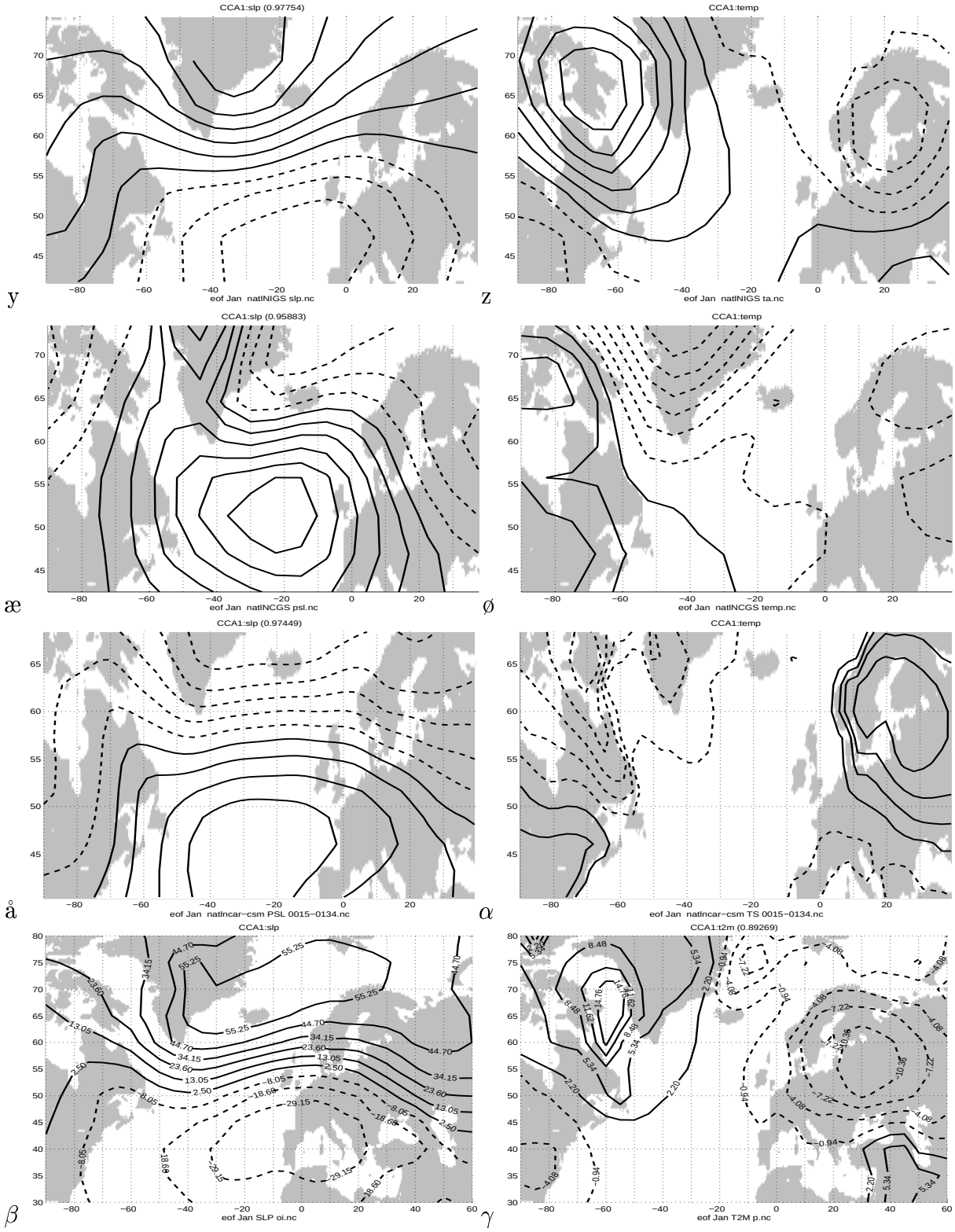

Figure 12: *The leading CCA SLP-Temperature patterns in various AOGCM results. Left: SLP, Right: near-surface temperature. The results are for CCSR/NIES (y,z), NCAR-DOE (æ,ø) NCAR CSM (å,α) and the* Benestad *(2000) historical analysis (β, γ).*

observations (β, γ). There is a small region east of Greenland in all the ensemble simulations where the temperature is correlated with the Scandinavian temperature. In comparison, the observations (β, γ) suggest strongest weighting for temperature over the Labrador Sea and the Baltics, and the SLP dipole has extensive northerly centre of action that covers Iceland, eastern Greenland, and the Norwegian Sea. But, the observations are not directly comparable to the model scenarios for reasons mentioned earlier. There are only small differences between the patterns of the various members of the ensemble. The SLP dipole centres of action are slightly displaced with respect to each other (c,e,g,i). The Azores anomaly in the first (c) and fourth member (i) is seen further east in the second (e) and third (g). The differences between the ensemble members give an indication about the robustness of these coupled patterns.

The SLP-T(2m) coupling in the CCCma ensemble (k-p) suggests less well-defined structures than in the HadCM2 model, although the CCA results bear a strong NAO signal and the large-scale structures are similar to the HadCM2 results. The CCCma results indicate stronger northerly geostrophic flow over the Labrador Sea associated with warm winters in northern Europe and low temperature over western Greenland. The maximum weights over the Baltics seen in the observations seem to be displaced to Scandinavia for the ensemble members 2 and 3 (n,p). The temperature weights over northern Europe in the ensemble member 1 (l) is distinct to the others, with weak weights over Norway and strong signal over eastern Russia. The eastern Greenland temperature is weakly correlated with those in northern Europe. The SLP dipole pattern suggests that the centres of action are more loosely tied to Iceland and the Azores. The differences between the ensemble members give an indication of the robustness of the analysis, as the same physical mechanism responsible for the SLP-temperature coupling. Thus the large differences between the temperature weights over northern Europe suggests a high level noise (the SLP and/or temperature affected by other factors than each other).

The CSIRO results (q,r) suggest a coupling between a SLP dipole pattern with centres of action located over Greenland and the Bay of Biscaya and temperature anomalies with similar polarity in the Nordic countries and over Greenland. There are only weak temperature weights over the Baltics. Thus, the SLP-T(2m) coupling in the CSIRO model does not involve the NAO much, but shows nevertheless an association with a north-south SLP dipole. Thus, this model may potentially have serious systematic errors associated with the simulation of the North Atlantic climate variability, and its downscaled results for this region should be interpreted with care.

The CCA results for the ECHAM3 model are given in Panels s and t of

Figure 12, and the results are similar to those of the CSIRO model, but with only eastern Greenland temperatures being correlated with the Scandinavian temperature.

The ECHAM4 results in panel u and v are more realistic, where the SLP dipole's northern centre of action is extends further east to Iceland and over the Greenland-Iceland-Norwegian Sea. The temperature field suggests that only in a small part of eastern Greenland is the temperature correlated with those in northern Europe. Again, this model may potentially contain systematic errors that can give misleading downscaling results for the North Atlantic region. However, this is difficult to tell, as with all the other model results, it is not possible to compare these CCA results with those of the historical analyses.

The CCA results for the GFDL model are shown in Figure 12w and x. The SLP dipole appears to be distorted with the southern centre of action located too far west and extending as far north as to Newfoundland. The corresponding temperature pattern suggests strongest weights over the Labrador Sea and the Baltics. Thus, although the SLP patterns appears to be skewed, the temperature field is closer to the observations (Figure 12γ) than those from the other models. However, the different SLP dipole structure may suggest of potential model biases that can affect any downscaling studies for the North Atlantic region.

The CCA results for the NCAR-DOE model are shown in æ and ø. Although the SLP weights exhibit a north-south dipole structure, these are quite different to the other CCA results. There is stronger SLP signal over western Greenland, and the associated temperature anomalies suggest only weak correlations over northern Europe. In contrast to the other results, the maximum temperature weights are found over Greenland.

The SLP-T(2m) coupling in the CCSR/NIES model is associated with strong SLP anomalies over Greenland and the Azores, but the northerly centre of action does not extend much east beyond Greenland. The CCA temperature field is realistic, but the European weights are displaced northwest of the observed location. Thus, there may potentially be some model bias in the CCSR/NIES model.

The coupled SLP-T(2m) pattern described by the NCAR CSM model (Figure 12å, α) bear a strong resemblance to the corresponding observations, suggesting that this model capable of giving a good description of advective processes.

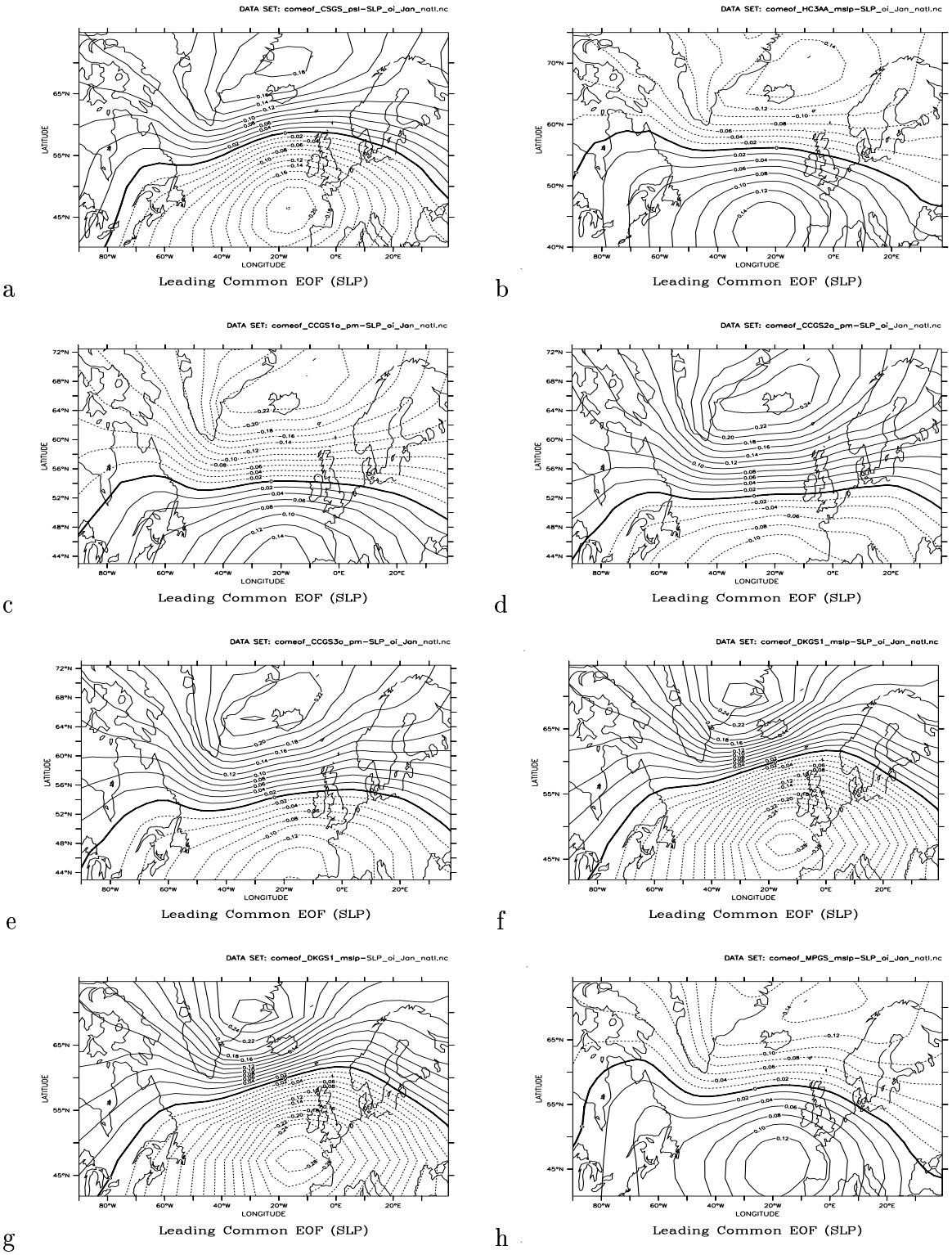

Figure 13: *The leading common EOF based on AOGCM SLP and* Benestad *(2000)OI SLP. The mean near-surface temperature (1.5-2m) fields from the converted AOGCM scenarios: a) CSIRO, b) HadCM3, c-f) 3 ensemble runs from CCCma, g) ECHAM3, and h) GFDL.*

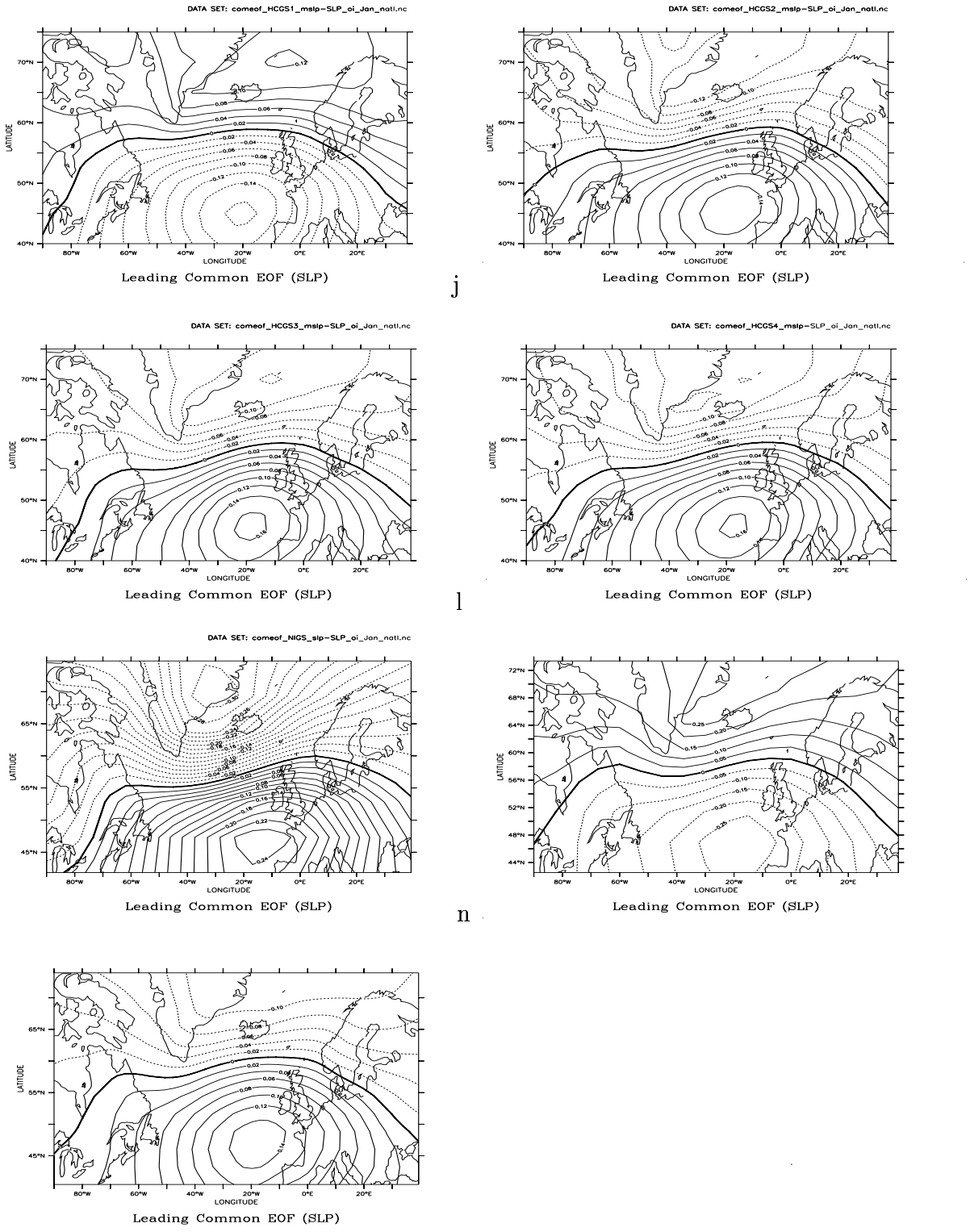

Figure 13: *The leading common EOF based on AOGCM SLP and* Benestad *(2000) OI SLP. The mean near-surface temperature (2m) fields from the converted AOGCM scenarios: i) ECHAM4, j-m) 4 HadCM2 runs, n) CCSR/NIES CGCM, o) NCAR CSM.*

3.8 Common EOF analysis of the SLP

The final set of analyses aims to identify normal SLP modes with the same geographical structure in the AOGCM results as in the historical analyses. The identification of such patterns is an important part of empirical downscaling, where historical large-scale climate anomalies are linked with local climate variations. One way to find such common spatial patterns is to apply a *common EOF* analysis (*Barnett*, 1999; *Benestad*, 1999c) to the model data and the historical SLP record.

Figure 13 shows the results from a common EOF analysis applied to the optimal interpolated January SLP of *Benestad* (2000) and corresponding SLP from the AOGCM. The polarity of these patterns shown here are arbitrary, as it doesn't matter whether the sense of the basis function (eigen vectors) is positive or negative.

All common EOFs show a north-south SLP dipole structure, with similar large-scale structures to the leading CCA patterns in section 3.7. The various EOF pattern differ in detail: some with stronger meridional SLP gradient (stronger zonal geostrophic wind, eg ECHAM3, GFDL, CCSR/NIES CGCM), and some with a southerly component to the geostrophic wind over the North Atlantic and Norwegian Sea (eg CSIRO, ECHAM3, GFDL, members 2-4 of HadCM2).

4 Conclusions

Most of the 14 AOGCM scenarios on the IPCC data site give a realistic description of the climate in the recent 50-years period, but there are some differences amongst the various models. The GFDL model does not give a realistic description of the past mean SLP, not its annual mean variance. The NCAR-DOE model describes a warmer world than was observed, and predicts higher temperatures than most of the other models. The NCAR-DOE model also gives a different account on the coupling between the SLP and near surface temperature over the North Atlantic than the other models and the historical analyses, but there may also be potential systematic errors in the CCCma, CSIRO and ECHAM3. The CCCma model describes substantially higher temperatures in the vicinity of Norway, as well as lower levels of variance. It also predicts a clear long-term trend towards more La Niña conditions (strengthened SOI) both for the past (1900-2000) and the future. The consistency among the ensemble members suggest that this trend is either due to the forcing or an artificial model drift. Because there has been no indication of such clear SOI trends in the real world, this discrepancy

may by indicative of CCCma model shortcomings. The CCSR/NIES model describes much higher level of variance over Scandinavia. Of all the models, the HadCM3, HadCM2, ECHAM4, and NCAR CSM results are the ones most similar to the historical observations, and these may therefore be the ones best suited for the use in empirical downscaling studies. The HadCM3 produces higher temperature variance in some regions than the other models, but the monthly mean temperature amplitudes diminish with time.

In areas where the NAO and ENSO play important roles for the local climate, local climate scenarios must be associated with a great deal of uncertainty because of the diverging accounts on the NAO and ENSO evolution. Some of these differences may be related to differences in the description of the coupling between dynamical thermodynamical climatic aspects revealed by CCA applied to SLP and temperature. It is nevertheless difficult to reconcile the diverging NAOI trends of the ECHAM4 model and HadCM2 from the CCA results alone, as both model gave a realistic reproduction of the SLP pattern coupled to the temperature field. It is furthermore difficult to explain the differences between NAOI and SOI the HadCM2 and CCCma ensembles in terms of these analyses alone, even though the HadCM2 seemed to give a more realistic reproduction of the past (1949-1998) climate. The NAO is important for the northern European climate, and it is expected that different conclusions may be drawn about the future depending on which model is used. It is therefore important to stress the dire need for a better understanding of the physical mechanisms behind the NAO.

As ENSO seems to have a marginal effect, if any, on the Norwegian climate, these differences may not be so important for our region. However, this case study also serves as an example of how dangerous it is to rely on just one AOGCM when making scenarios for the future climate. Furthermore, the effects of ENSO does affect Norway indirectly in economical terms.

5 Appendix

References

Barnett, T.P. 1999. Comparison of Near-Surface Air Temperature Variability in 11 Coupled Global Climate Models. *Journal of Climate*, **12**, 511–518.

Benestad, R. E. 2000. *Analysis of gridded sea level pressure and 2-meter temperature for 1873-1998 based on UEA and NCEP re-analysis II.* KLIMA 03/00. DNMI, PO Box 43 Blindern, 0313 Oslo, Norway.

Benestad, R.E. 1998. *CCA applied to Statistical Downscaling for Prediction of Monthly Mean Land Surface Temperatures: Model Documentation.* Klima 28/98. DNMI, PO Box 43 Blindern, 0313 Oslo, Norway.

Benestad, R.E. 1999a. *Conversion and quality control of the ECHAM4/OPYC3 GSDIO data to the netCDF format and a brief introduction to Ferret.* KLIMA 27/99. DNMI, PO Box 43 Blindern, 0313 Oslo, Norway.

Benestad, R.E. 1999b. *Conversion of the NCEP re-analysis data to the netCDF format and quality control.* KLIMA 31/99. DNMI, PO Box 43 Blindern, 0313 Oslo, Norway.

Benestad, R.E. 1999c. *Evaluation of the common EOF approach in linear Empirical Downscaling of Future ECHAM4/OPYC3 GSDIO Climate Scenarios.* KLIMA 35/99. DNMI, PO Box 43 Blindern, 0313 Oslo, Norway.

Benestad, R.E. 2001. The cause of warming over Norway in the ECHAM4/OPYC3 *GHG* integration. *International Journal of Climatology*, **21**, 371–387.

Boer, G.J., Flato, G.M., Reader, M.C., & Ramsden, D. 1998a. A transient climate change simulation with historical and projected greenhouse gas and aerosol forcing: experimental design and comparison with the instrumental record for the 20th century. *Climate Dynamics.*

Boer, G.J., Flato, G.M., Reader, M.C., & Ramsden, D. 1998b. A transient climate change simulation with historical and projected greenhouse gas and aerosol forcing: projected climate for the 20th century. *Climate Dynamics.*

Boville, B. A., & Gent, P. R. 1998. The NCAR Climate System Model, Version One. *Journal of Climate*, **11**(6).

Collins, M. 2000. The El Niño-Southern Oscillation in the Second Hadley Centre Coupled Model and Its Repsonse to Greenhouse Warming. *Journal of Climate.*

Cullen, M.J.P. 1993. The unified forecast/climate model. *Meteor. Mag.*, 81–94.

Dey, C.H. 1998. *GRIB*. 1 edn. NCEP Central Operations/NOAA. Office note 388.

Emori, S., Nozawa, T., Abe-Ouchi, A., Numaguti, A., Kimoto, M., & Nakajima, T. 1999. Coupled ocean-atmosphere model experiments of future climate change with an explicit representation of sulfate aerosol scattering. *Journal of the Meteorological Society of Japan*, **77**(6), 1299 –1307.

Gordon, H. B., & O'Farrell, S. P. 1997. Transient climate change in the CSIRO coupled model with dynamic sea ice. *Monthly Weather Review*, **125**, 875– 907.

Jones, P.D., Jonsson, T., & Wheeler, D. 1997. Extension to the North Atlantic Oscillation using early instrumental pressure observations from Gibraltar and South-West Iceland. *International Journal of Climatology*, **17**, 1433–1450.

Kapala, A., Mächel, H., & Flohn, H. 1998. Behaviour of the centres of action above the Atlantic since 1881. Part II: Associateion with regional climate anomalies. *International Journal of Climatology*, **18**, 22–36.

McFarlane, N.A., Boer, G.J., Blanchet, J.-P., & Lazare, M., J. 1992. *Climate*.

Rew, R., Davis, G., Emmerson, S., & Davies, H. 1996. *NetCDF User's Guide*. Unidata Program Center.

S.Hankin, & Denham, M. 1994. *Ferret Users Guide*. NOAA/PMEL/TMAP.